Inorganic Chemistry

pubs.acs.org/IC

Article

Selective Oxidation by $H_5[PV_2Mo_{10}O_{40}]$ in a Highly Acidic Medium

Chandan Kumar Tiwari, Mark Baranov, Alevtina Neyman, Ronny Neumann, and Ira A. Weinstock*

Cite This: *Inorg. Chem.* 2020, 59, 11945−11952

Read Online

ACCESS | Metrics & More | Article Recommendations | Supporting Information

ABSTRACT: Dissolution of the polyoxometalate (POM) cluster anion $H_5[PV_2Mo_{10}O_{40}]$ (**1**; a mixture of positional isomers) in 50% aq H_2SO_4 dramatically enhances its ability to oxidize methylarenes, while fully retaining the high selectivities typical of this versatile oxidant. To better understand this impressive reactivity, we now provide new information regarding the nature of **1** (115 mM) in 50% (9.4 M) H_2SO_4. Data from ^{51}V NMR spectroscopy and cyclic voltammetry reveal that as the volume of H_2SO_4 in water is incrementally increased to 50%, V(V) ions are stoichiometrically released from **1**, generating two reactive pervanadyl, VO_2^+, ions, each with a one-electron reduction potential of ca. 0.95 V (versus Ag/AgCl), compared to 0.46 V for **1** in 1.0 M aq H_2SO_4. Phosphorus-31 NMR spectra obtained in parallel reveal the presence of PO_4^{3-}, which at 50% H_2SO_4 accounts for all the P(V) initially present in **1**. Addition of $(NH_4)_2SO_4$ leads to the formation of crystalline $[NH_4]_6[Mo_2O_5(SO_4)_4]$ (34% yield based on Mo), whose structure (from single-crystal X-ray diffraction) features a corner-shared, permolybdenyl $[Mo_2O_5]^{2+}$ core, conceptually derived by acid condensation of two MoO_3 moieties. While **1** in 50% aq H_2SO_4 oxidizes *p*-xylene to *p*-methylbenzaldehyde with conversion and selectivity both greater than 90%, reaction with VO_2^+ alone gives the same high conversion, but at a significantly lower selectivity. Importantly, selectivity is fully restored by adding $[NH_4]_6[Mo_2O_5(SO_4)_4]$, suggesting a central role for Mo(VI) in attenuating the (generally) poor selectivity achievable using VO_2^+ alone. Finally, ^{31}P and ^{51}V NMR spectra show that intact **1** is fully restored upon dilution to 1 M H_2SO_4.

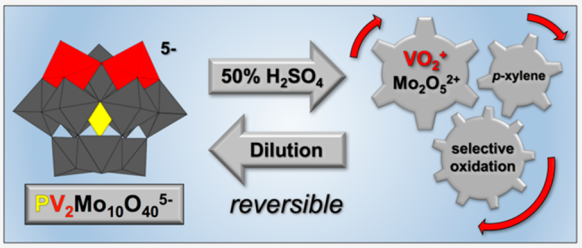

INTRODUCTION

The molybdovanadophosphate cluster anion, $H_5[PV_2Mo_{10}O_{40}]$ (**1**), is a versatile catalyst for selective aerobic oxidations of organic and inorganic compounds via a range of mechanisms, from electron transfer (ET) to electron-transfer induced oxygen transfer (ET-OT), a homogeneous liquid-phase analogue of Mars−van Krevelen type reactions.[1−4] Over the past three decades, numerous advances have been achieved using **1** in a range of solvents, including water, MeCN, and toluene, with reduced forms of **1** reoxidized by air/O_2.[3,5,6] In general, high selectivities have been attributed at least in part to the stabilization or ET sequestration of organic-radical intermediates by **1** itself, and during reoxidation, the absence of reactive intermediates from the partial reduction of O_2 that, if generated as they are in numerous aerobic oxidations, would give rise to nonselective radical-chain processes.

When functioning as an outer-sphere oxidant, the activity of **1** is controlled by its reduction potential, which at 0.4−0.45 V versus the saturated calomel electrode (SCE) has historically restricted its ET activity to transformations of more readily oxidizable substrates.[1,2] This situation changed dramatically upon discovery that in 80% aq H_2SO_4 the reduction potential of **1** increased to 1.1−1.2 V, facilitating its use in transforming carbohydrates to synthesis gas.[7] In 50% aq H_2SO_4, **1** (92 mM) is capable of oxidizing benzene, facilitating its aerobic oxidation to phenol,[8] and 115 mM solutions of **1** selectively convert methylarenes to benzaldehyde derivatives.[9]

While the protonation of intact **1** in 50% (9.4 M) aq H_2SO_4 could readily account for the more positive reduction potential observed in that solvent system,[8,9] the retention of high selectivity further suggested that the cluster anion remained otherwise largely intact and thus able to sequester electrons from radical-organic intermediates. Consistent with this, after the reaction, electrochemical reoxidation, and dilution in D_2O, ^{31}P NMR spectra invariably revealed the signature set of signals associated with the five positional isomers of $H_5PV_2Mo_{10}O_{40}$.[7−9]

To better understand its reactivity and selectivity, the nature of **1** (115 mM) in 50% aq H_2SO_4 has now been systematically investigated by ^{51}V and ^{31}P NMR spectroscopy, ESR spectroscopy, cyclic voltammetry (CV), and single-crystal X-ray crystallography and by a series of reactions involving oxidation of a model substrate, *p*-xylene, to *p*-methylbenzaldehyde. The herein reported data, which provide an entirely new picture of **1** in 50% aq H_2SO_4, reveal the reversible formation

Received: December 29, 2019
Published: March 5, 2020

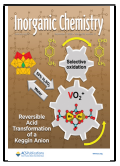

https://dx.doi.org/10.1021/acs.inorgchem.9b03747
Inorg. Chem. 2020, 59, 11945−11952

of a selective oxidative system composed of free VO_2^+ (for enhanced reactivity), with high selectivity attributed to the coformation of an oxo-bridged (corner-sharing) dimeric permolybdenyl cation, $[Mo_2O_5]^{2+}$ (Figure 1). Control experi-

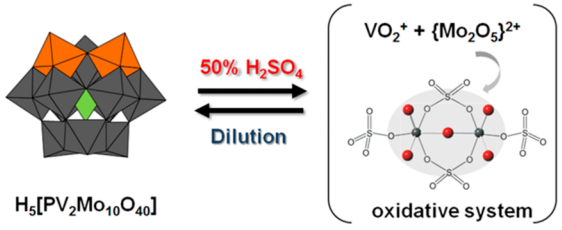

Figure 1. $H_5[PV_2Mo_{10}O_{40}]$ (**1**) in 50% aq H_2SO_4. Dissolution of **1** (at left) in this acidic medium generates highly reactive pervanadyl ions, VO_2^+, along with a $[Mo_2O_5]^{2+}$-core complex (at right), shown below to be responsible for retention of selectivity. Dilution to 1 M H_2SO_4 leads to a quantitative reconstitution of intact **1**.

ments indicate that free phosphate (also observed) plays a minimal role. As previously observed,[7−9] dilution of this thermodynamically stable oxidative system leads quantitatively to hydrolytic self-assembly of the component species into fully intact **1**.

RESULTS AND DISCUSSION

To investigate the solution-state chemistry of **1** in 50% aq H_2SO_4, the first set of experiments involved the use of ^{51}V NMR spectroscopy, in combination with cyclic voltammetry, to help explain the previously observed[9] ca. 0.5 V increase in reduction potential.

For this, ^{51}V NMR spectra of **1** (115 mM) were obtained for solutions containing incrementally larger concentrations of H_2SO_4. The use of 115 mM **1** was critically important not only because this concentration was used in previously reported reactivity studies[9] but also because of the speciation chemistry of metal cations, including those that form metal-oxide cluster anions (POMs) is a function of concentration.[10,11] As such, smaller concentrations of **1** would not provide definitive information about the reactive system under investigation.

Release of Pervanadyl Ions (VO_2^+). The pH of 115 mM **1** in pure water is 0.06. As the concentration of H_2SO_4, $[H_2SO_4]$, was incrementally increased from 0 to 5 M, the set of ^{51}V NMR signals characteristic of the five positional isomers of **1**, observed between −510 and −525 ppm, decreased in intensity and were entirely replaced by a broad signal at ca. −550 ppm (Figure 2). This signal shifted to more negative ppm values as $[H_2SO_4]$ was increased to 9.4 M. Notably, very little change was observed when an additional 0.25 equiv (28.75 mM) of $NaVO_3$ was added (topmost plot in Figure 2). Moreover, an identical solvent system containing 230 mM $NaVO_3$ gave a ^{51}V NMR spectrum nearly identical to that obtained upon dissolution of **1** (Figure S1). The sharp signal at −539 ppm, indicated by an asterisk in Figure 2, is due to the external reference, $K_4[PVW_{11}O_{40}]$, present in a coaxial NMR tube.

The nearly identical spectrum of $NaVO_3$ suggested that as $[H_2SO_4]$ increased, V(V) ions were released from **1** to give pervanadyl ions, VO_2^+. Although documented for much smaller concentrations of **1** in 1−3 M acid, the partial release of V(V) from **1** has been observed in equilibrium with a proposed V-depleted anion, $[PVMo_{10}O_{39}]^{8-}$.[12] In the present case, using 9.4 M H_2SO_4, the ^{51}V NMR data suggested a more

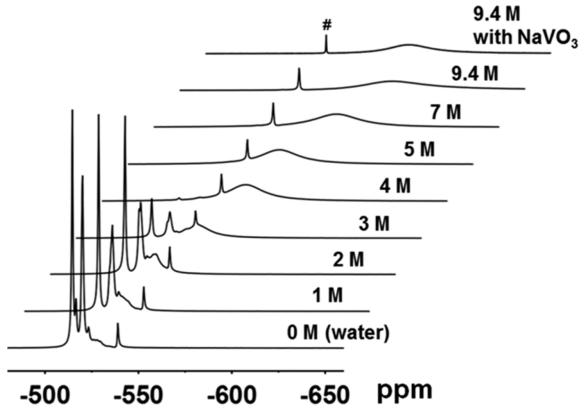

Figure 2. Vanadium-51 NMR spectra of 115 mM **1** as $[H_2SO_4]$ was increased from 0 to 9.4 M (50% v/v). The measurements were carried out using $K_4[PVW_{11}O_{40}]$ (0.1 equiv with respect to **1** in 9:1 H_2O:D_2O; indicated by a hash-tag, #) as an external reference in a coaxial NMR tube. The topmost spectrum was obtained after adding an additional 0.25 equiv of $NaVO_3$ in 9.4 M H_2SO_4.

extensive loss of V from **1**. However, due to the broad signals associated with the quadrupolar ^{51}V nucleus ($I = 7/2$), and the possibility of dynamic processes (such as reversible protonation) leading to signal broadening, no definitive conclusions could be reached without independently quantifying the extent of V release. This was done by the cyclic voltammetric analysis of the same set of solutions as shown in Figure 2, after which the number of equivalents of VO_2^+ released was quantified by amperometric titration.

First, cyclic voltammograms (CVs) were obtained as a function of $[H_2SO_4]$ (Figure 3A). These revealed a large

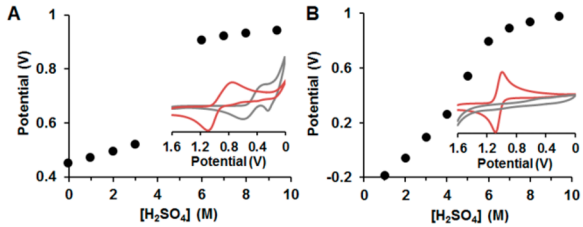

Figure 3. (A) Reduction potentials as a function of $[H_2SO_4]$ for 115 mM **1**. Inset: the CV of **1** in 0.1 M H_2SO_4 (gray curve; for clarity, the *y*-axis has been suppressed by a factor of 3) and in 9.4 M H_2SO_4 (red curve). (B) Reduction potentials as a function of $[H_2SO_4]$ for 230 mM $NaVO_3$ (from 1 to 5 M H_2SO_4, cathodic-maxima values were used; see Figure S3). Inset: the CV of $NaVO_3$ in pure water (gray curve) and in 9.4 M H_2SO_4 (red curve).

positive shift in reduction potential as $[H_2SO_4]$ increased from 3 to 4 M. (Between these concentrations, broad voltammograms were obtained;[9] see Figure S2.) Notably, this shift in reduction potential corresponds nicely with the $[H_2SO_4]$ values at which large changes were observed by ^{51}V NMR spectroscopy (Figure 2). In the inset to Figure 3A, CVs obtained at 0 and 9.4 M H_2SO_4 are shown as gray and red plots, respectively.

For comparison, CVs were also obtained as a function of $[H_2SO_4]$ for $NaVO_3$ alone (Figure 3B). A similar positive shift in reduction-potential values was observed. In the absence of simultaneous speciation chemistry of **1**, a smoother shift to more positive potentials was observed. In both cases, however, the magnitudes of the positive shifts and the final potentials

https://dx.doi.org/10.1021/acs.inorgchem.9b03747
Inorg. Chem. 2020, 59, 11945−11952

were similar. In 9.4 M H_2SO_4, the CV of pure $NaVO_3$ (red curve in the inset to Figure 3B) was electrochemically reversible, while quasi-reversible behavior was observed for V from **1**, pointing to some interactions between released VO_2^+ and other products of the speciation of **1**.

Amperometric titration was then used to quantify the numbers of equivalents of VO_2^+ released from **1** upon dissolution in 9.4 M H_2SO_4. For this, **1** (115 mM) was dissolved in the acidic medium and the cathodic-current maximum was used as a starting point for the titration (blue curve in Figure 4A). Next (also in Figure 4A) CVs were

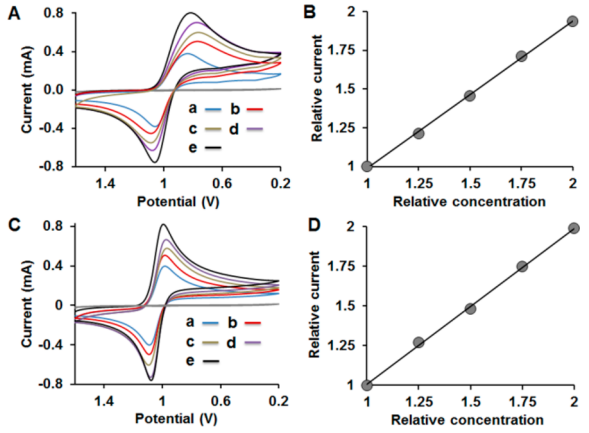

Figure 4. (A) Amperometric titration of V(V) released from 115 mM **1** (i.e., 230 mM V(V) in 9.4 M H_2SO_4) by incremental additions of $NaVO_3$ as follows: (a) 0 mM (i.e., **1** alone), (b) 57.5 mM, (c) 115 mM, (d) 172.5 mM, and (e) 230 mM. (B) Plot of cathodic-current maxima relative to that for **1** (i.e., (a) in panel A) as a function of the total concentration of V(V) relative to that from **1**. (C) Amperometric titration of 230 mM$NaVO_3$ (in 9.4 M H_2SO_4) by incremental additions of more $NaVO_3$ to give the following total concentrations: (a) 230 mM, (b) 287.5 mM, (c) 345 mM, (d) 402.5 mM, and (e) 460 mM. (D) Plot of cathodic-current maxima relative to that for 230 mM $NaVO_3$ (i.e., (a) in panel C) as a function of the total concentration of V(V) relative to 230 mM.

recorded after incremental additions of $NaVO_3$, up to 230 mM added VO_3^- (i.e., identical to the total concentration of V(V) in 115 mM **1**). As VO_3^- was added, the cathodic current relative to that for **1** alone doubled from unity (for **1** alone) to two, as the "relative concentration" of free V(V) increased from 230 mM (from **1** alone) to a total of 460 mM (Figure 4B). This doubling of current indicated that upon dissolution of 115 mM **1** in 9.4 M H_2SO_4, both V(V) atoms are released to form VO_2^+.

To further confirm the fidelity of this method, a similar experiment was carried out starting with a solution of 230 mM VO_3^- (Figure 4C,D). An identical doubling of the relative current (Figure 4D) confirmed that no unexpected concentration-dependent behavior was responsible for the results shown in Figure 4A,B.

Release of Phosphate. The solution-state behavior of the phosphate heteroatom in **1** as a function of [H_2SO_4] was then investigated by ^{31}P NMR spectroscopy (Figure 5). As was observed in ^{51}V NMR spectra (Figure 2), the intensity of the characteristic set of signals associated with positional isomers of **1** decreased with [H_2SO_4], while the intensity of a new (broad) signal closer to 0 ppm grew correspondingly. Signals in this region, near 0 ppm, are typical for solutions of phosphate. At the largest [H_2SO_4] values, three broad signals

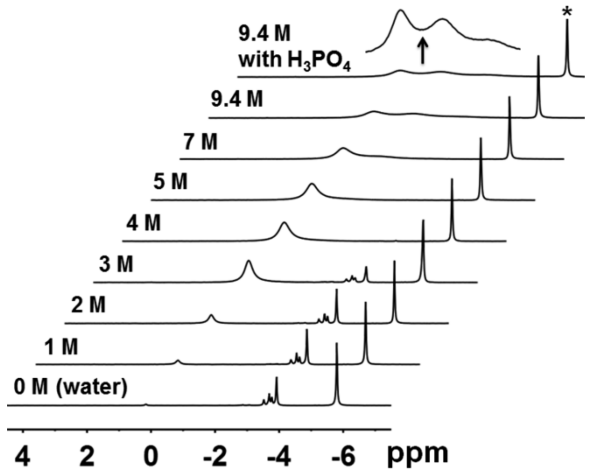

Figure 5. Phosphorus-31 NMR spectra of **1** (115 mM) at incrementally larger [H_2SO_4] values. The measurements were carried out using $Na_4P_2O_7$ in 90:10 v:v H_2O:D_2O as a quantitative integration standard (*; 0.33 equiv with respect to **1**) in a coaxial NMR tube.

were observed. Integration using a coaxial tube containing $Na_4P_2O_7$ as an external standard (sharp signal at −5.8 ppm in Figure 5) indicated a quantitative release of phosphate.

The intensity of the broad signals increased when an additional 0.25 equiv (28.75 mM) of H_3PO_4 was added, but no new signals were observed (see the two topmost spectra in Figure 5). Given that ^{31}P is a spin $^1/_2$ nucleus (giving narrow-line width signals), and in light of the absence of paramagnetic species, the broadness of the ^{31}P NMR signals suggested the presence of a dynamic process involving relatively labile species.

This was explored further by preparing 9.4 M H_2SO_4 solutions of H_3PO_4 alone and in combination with $NaVO_3$ (plots a and b, respectively, in Figure 6A). In both cases,

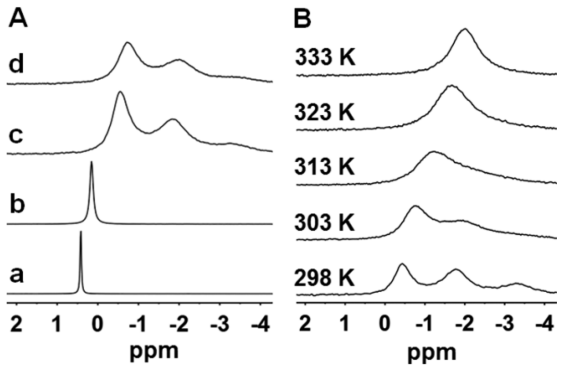

Figure 6. (A) Phosphorus-31 NMR spectra (in 9.4 M H_2SO_4) of (a) 115 mM H_3PO_4, (b) 115 mM H_3PO_4 and 230 mM $NaVO_3$, (c) 115 mM H_3PO_4 and 1150 mM Na_2MoO_4, and (d) 115 mM **1**. (B) Variable-temperature ^{31}P NMR spectra of **1** in 50% H_2SO_4, showing coalescence at 333 K.

relatively sharp ^{31}P NMR signals were observed near 0 ppm. When H_3PO_4 was combined with 10 equiv of Na_2MoO_4, however, three broad signals, similar to those observed for **1**, were observed (plots c and d, respectively, in Figure 6A).

This suggested that the broad ^{31}P NMR signals were due to a dynamic process involving both P and Mo. The dynamic nature of the system was confirmed by variable-temperature

https://dx.doi.org/10.1021/acs.inorgchem.9b03747
Inorg. Chem. 2020, 59, 11945−11952

^{31}P NMR spectroscopy (Figure 6B). As the temperature of a solution of **1** in 9.4 M H_2SO_4 was increased from 298 to 333 K, the three broad signals coalesced.

Reactivity and Selectivity. The above spectroscopic and electrochemical data pointed to the formation of a new set of species upon dissolution of **1** in 9.4 M H_2SO_4. Although the increase in reactivity relative to **1** in pure water or organic solvents could be explained by the quantitative formation of $V^VO_2^+$, the pervanadyl cation is known to give only modest selectivities. This raised the intriguing question as to why the constellation of species present in 9.4 M H_2SO_4 retained the high selectivity characteristic of ET-driven oxidations by **1**.

This was addressed using the ET oxidation of an arylalkane to the corresponding benzaldehyde.[9] For this, *p*-xylene was chosen as a representative substrate. Its conversion to *p*-methylbenzaldehyde (eq 1) was investigated by comparing the reactivity and selectivity of **1** with solutions of its component species in 9.4 M H_2SO_4 (Figure 7).

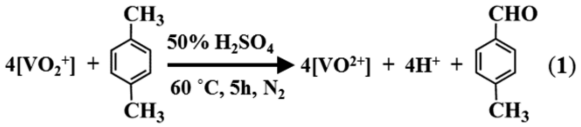

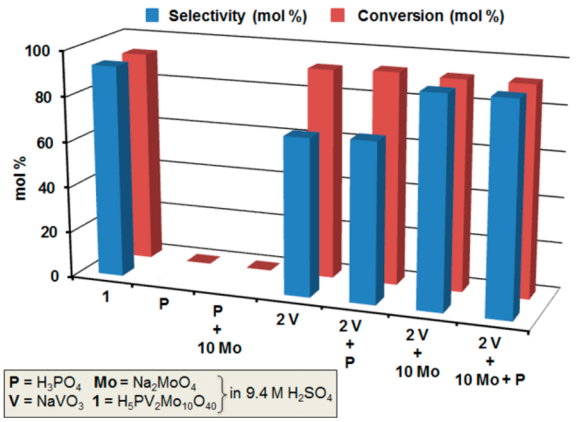

Figure 7. Conversion and selectivity for oxidations of *p*-xylene in 9.4 M H_2SO_4. Species added to the acidic medium, defined in the key at lower left, are abbreviated below the *x*-axis as equivalents added relative to 115 mM **1**, i.e., P = 115 mM H_3PO_4, 2 V = 230 mM $NaVO_3$, and 10Mo = 1150 mM Na_2MoO_4. In each case, *p*-xylene, 1.84 mmol (0.168 g), was layered on top of 8 mL of 9.4 M H_2SO_4 in a high-pressure vessel and kept at 60 °C for 5 h under N_2.

The percent conversion (mol % relative to V) and selectivity (mol % *p*-methylbenzaldehyde relative to other products) for the reaction of **1** (115 mM in 9.4 M H_2SO_4) is shown at the far left in Figure 7.

The high conversion with high selectivity is in line with previously reported data for this reaction.[9] The experiments then listed from left to right in Figure 7, all in 9.4 M H_2SO_4, were designed to systematically elucidate the species responsible for the high reactivity and selectivity. In the absence of V, i.e., for H_3PO_4 alone (P), and in combination with 10 equiv of Na_2MoO_4 (P + 10Mo), no reactivity was observed. For 2 equiv of $NaVO_3$ alone (2 V) or in combination with H_3PO_4 (2 V + P), high conversions were achieved, but with compromised selectivity relative to **1**. However, when Na_2MoO_4 was added to $NaVO_3$ (2 V + 10Mo,) selectivity was fully restored, i.e., identical to that obtained using **1**. The same results were obtained when H_3PO_4 was included (2 V + 10Mo + P), indicating that the dynamic species observed by ^{31}P NMR for combinations of H_3PO_4 and Na_2MoO_4 (Figure 6) were not essential to the retention of selectivity.

Upon reduction by *p*-xylene, the color of the solution changed from orange-red to greenish-blue. To further confirm the central role of VO_2^+ as the electron acceptor, the reduced (greenish-blue) solution was analyzed by ESR spectroscopy. The results (Figures S4–S6, Table S1) are definitive for the formation of vanadyl ion, $V^{IV}O^{2+}$, rather than for the (hypothetical) presence of reduced **1**. Taken alone, this result does provide definitive evidence for extensive rearrangement of **1**. This is because the reduction of V(V) to V(IV) in **1** is known to induce the release of V(IV) ions from the otherwise intact Keggin-POM structure. Nevertheless, ESR identification of $V^{IV}O^{2+}$ is consistent with the release of reactive pervanadyl, $V^VO_2^+$, ions upon dissolution of **1** in 9.4 M H_2SO_4.

Additional support for conversion of **1** into constituent species in 9.4 M H_2SO_4 was provided by investigating solutions of related molybdovanadophosphates, $H_4[PVMo_{11}O_{40}]$ and $H_6[PV_3Mo_9O_{40}]$. In 9.4 H_2SO_4, both cluster anions gave ^{31}P and ^{51}V NMR spectra and electrochemical data very similar to those provided in Figures 2, 3, and 5 (see Figures S7–S8). Moreover, data from amperometric titrations (cf. Figure 4), indicated 1 and 3 equiv of $V^VO_2^+$, respectively, were released from the mono- and trivanadium cluster anions (Figures S9 and S10). As expected, 9.4 M H_2SO_4 solutions containing $H_4[PVMo_{11}O_{40}]$ (230 mM; 2 equiv relative to **1** in Figure 7) or of $H_6[PV_3Mo_9O_{40}]$ (76.7 mM; two-thirds of an equivalent relative to **1**), gave conversions of *p*-xylene effectively identical to that shown in Figure 7 for **1**, and with equally good selectivities (Figure S11). Notably, the first one-electron reduction potentials of $H_4[PVMo_{11}O_{40}]$ and $H_6[PV_3Mo_9O_{40}]$ are, respectively, more and less positive compared with that of **1** (Figure S12). Nevertheless, once the stoichiometry of $V^VO_2^+$ is taken into account, the three cluster anions display identical reactivities and selectivities.

Formation of $[Mo_2O_5]^{2+}$. The results in Figure 7 identify the presence of Mo(VI) as critical to the high selectivity observed for ET oxidations by **1** in 50% H_2SO_4. As such, evidence for the solution-state structure of molybdate in this medium was sought. As NMR spectra of Mo nuclei are relatively uninformative, an effort was made to obtain crystals of Mo-containing species from 9.4 M H_2SO_4. However, solutions of **1** gave considerable amounts of pervanadyl phosphate and pervanadyl sulfate, making it difficult to isolate crystalline Mo-based species. Therefore, Na_2MoO_4 was dissolved in H_2SO_4, with the concentration of Mo (1150 mM) equal to that in 115 mM **1**. To isolate the crystalline product, ammonium sulfate, $(NH_4)_2SO_4$, which is highly soluble in 9.4 M H_2SO_4, was added.

Crystals of $[NH_4]_6[Mo_2O_5(SO_4)_4]$ (**2**; 34% yield based on Mo), were obtained and characterized by single-crystal X-ray diffraction. The complex (Figure 8) features a corner-shared $[Mo_2O_5]^{2+}$ core, conceptually derived by acid condensation of two MoO_3 moieties.

As shown in eq 2, MoO_3 (or its hydrated form) is prepared by dissolving MoO_4^{2-} in strong aqueous acid, e.g., 1 M $HClO_4$.[13] In 9.4 M H_2SO_4, reaction with an additional 1 equiv of H^+ per Mo gives the $[Mo_2O_5]^{2+}$ core of **2** (eq 3).

https://dx.doi.org/10.1021/acs.inorgchem.9b03747
Inorg. Chem. 2020, 59, 11945–11952

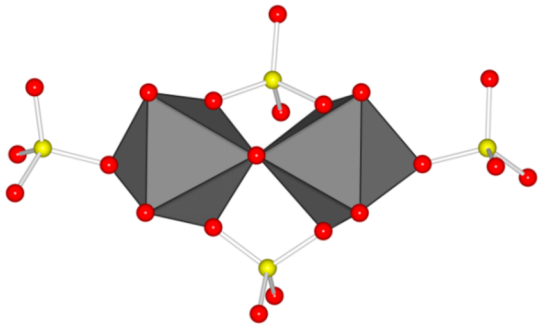

Figure 8. Crystal structure of $[NH_4]_6[Mo_2O_5(SO_4)_4]$ (**2**). The polyhedra represent six-coordinate MoO_6 units, while terminal and bridging SO_4^{2-} ligands are shown in ball and stick notation, with O in red and S in yellow.

$$MoO_4^{2-} + 2H^+ = MoO_3 + H_2O \quad (2)$$

$$2MoO_3 + 2H^+ = [Mo_2O_5]^{2+} + H_2O \quad (3)$$

Notably, the corner-shared Mo_2O_5 core of **2** is a feature of several reported molybdo-organic complexes.[14−20] Similar to those metalloorganic complexes, **2** possesses a *syn*-$[Mo_2O_5]^{2+}$ unit with a 2-fold axis of rotation passing through the corner-shared O atom. The bond lengths of the terminal Mo=O ligands of **2** (1.68−1.69 Å) are in good agreement with Mo=O bond lengths reported for the related molybdo-organic complexes (1.68−1.71 Å).[17] Distances from the corner-shared O atom to the Mo centers in **2** (1.89 and 1.90 Å) are also in line with the reported value of 1.88 (i.e., for both distances).[17] A complete set of lengths and angles is given in Figure S13 and Tables S2−S4.

At the same time, to our knowledge, the permolybdenyl core, $[Mo_2O_5]^{2+}$, of **2** has not been identified as a product of condensation in aqueous acid. In this context, **2** may be viewed as a new member in the natural progression from titanyl, $[Ti^{IV}O]^{2+}$, to pervanadyl $[V^{V}O_2]^{+}$, to permolybdenyl, $[Mo^{VI}_2O_5]^{2+}$, oxy cations.

Evidence for the latter species in actual solutions of **1** was sought by dissolving **2** and H_3PO_4 in 9.4 M H_2SO_4 and analyzing the solution by ^{31}P NMR. The mixture (Figure 9; bottom) gave rise to three broad signals, very similar to those observed for **1** itself (topmost spectrum in Figure 9).

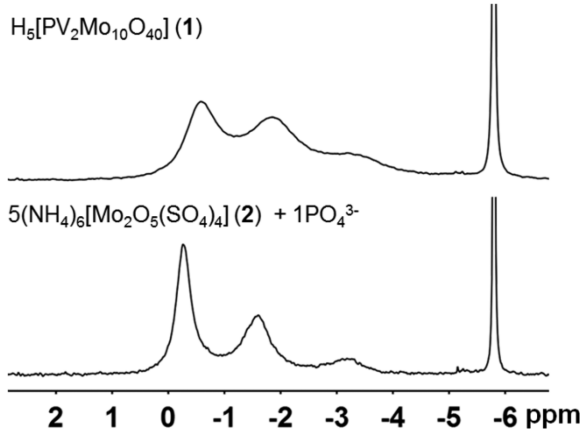

Figure 9. P-31-NMR spectra in 9.4 M H_2SO_4 of H_3PO_4 and **2** (1:10 ratio of P to Mo; bottom) and of **1** (top).

This finding is consistent with the dissolution of **1** in 9.4 M H_2SO_4 giving rise to a dynamic equilibrium involving interactions between phosphate and **2**.

Nevertheless, the data in Figure 7 point to Mo-based species alone as sufficient for retaining the high selectivity of **1**. In this regard, selectivity in ET oxidations by **1** is in many cases attributed to the rapid sequestration of organic radicals by additional equivalents of V(V) in the intact POM itself. In the present case, a similar selectivity-enhancing mechanism could involve the oxidation of radical intermediates by the $[Mo_2O_5]^{2+}$ core of **2**, alone, or with phosphate anions in rapid exchange with SO_4^{2-} ligands. The impressive reactivity of $H_5PV_2Mo_{10}O_{40}$ (**1**; 115 mM) in 9.4 M H_2SO_4[8,9] thus arises from the presence of pervanadyl ions, VO_2^+ (with a reduction potential of 0.95 V versus Ag/AgCl), while selectivity is apparently provided by a dynamic mixture of complexed dimolybdenum(VI) oxide, $[Mo_2O_5]^{2+}$ cations. While CVs attributable to Mo(VI) in 9.4 M H_2SO_4 (from **1**, as well as from **2**), are poorly defined, cathodic responses occur over a range of negative potentials, from ca. 0 to −0.4 V (Figure S14). While **2** alone does not oxidize *p*-xylene to *p*-methylbenzaldehyde (Figure S11), the Mo-containing species are nevertheless sufficiently reactive to provide for high selectivity by sequestering electrons from organic-radical intermediates.

Reversible Formation of a Multicomponent System for Selective Electron-Transfer Oxidation. The ^{31}PNMR spectrum of **1** (40 mM) at its native pH of 0.8 is shown at the bottom of Figure 10A. Data provided above show that in 50%

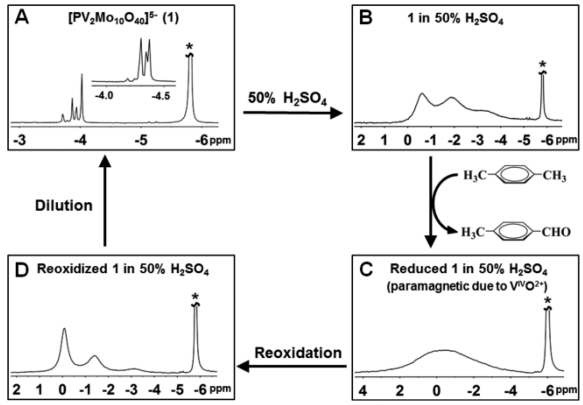

Figure 10. $H_5[PV_2W_{10}O_{40}]$ (**1**) in 9.4 M H_2SO_4. The four panels show ^{31}P NMR spectra (A) of 40 mM **1** in pure water (native pH = 0.8), (B) of 115 mM **1** in 9.4 M H_2SO_4, (C) of the same solution after reduction by *p*-xylene, (D) after electrochemical reoxidation, and (inset to part A) after dilution of the reoxidized solution to 40 mM, along with addition of NaOH to increase the pH to 0.8.

(9.4 M) aq H_2SO_4, $H_5PV_2Mo_{10}O_{40}$ (**1**; 115 mM) undergoes condensation-driven rearrangement to form aqua and/or sulfate complexed pervanadyl (VO_2^+) and permolybdenyl ($[Mo_2O_5]^{2+}$) cations (eq 4; its ^{31}PNMR spectrum is shown in Figure 10B).

$$H_5[PV_2Mo_{10}O_{40}]\ (\mathbf{1}) + 9H^+ = PO_4^{3-} + 2VO_2^+ + 5[Mo_2O_5]^{2+} + 7H_2O \quad (4)$$

These species act in concert to provide high reactivity and selectivity (Figure 10B,C). A ^{31}PNMR spectrum of the reduced solution is shown in Figure 10C. Importantly, ESR spectra (Figures S4−S6, Table S1) confirm the reduced species

https://dx.doi.org/10.1021/acs.inorgchem.9b03747
Inorg. Chem. 2020, 59, 11945−11952

is the vanadyl ion, $V^{IV}O^{2+}$, whose spectrum is distinct from that of reduced **1** (i.e., $H_6PV^{IV}V^{V}Mo_{10}O_{40}$).[21] Electrochemical reoxidation (bulk electrolysis) gives a solution with the ^{31}P NMR spectrum shown in panel D, very similar to that acquired before *p*-xylene oxidation (panel B).

In polyoxometalate chemistry, as in aqueous speciation chemistry generally, the acid condensation that occurs upon dissolution of **1** in 50% H_2SO_4 is reversible. Upon dilution and NaOH neutralization of the solution in panel D (115 mM **1** in 50% H_2SO_4) to 40 mM (pH 0.8), *hydrolysis-driven* assembly (the reverse of eq 4) leads to the complete re-formation of **1**, as shown by the ^{31}P NMR spectrum provided as an inset in the center of panel A. The shift in ppm values associated with the positional isomers of **1** is due to the presence of Na_2SO_4 (3.2 M).[22]

Unique Medium for Cluster-Anion Formation and Reactivity. Viewed from a general perspective of polyoxometalate synthesis, 50% aq H_2SO_4 is a unique environment. POMs are typically formed by stoichiometric reactions of metalate anions (e.g., MO_4^{2-}, M = Mo(VI) or W(VI)), or their partially condensed cluster anion forms, with mineral acids in water. Once the ratio of H^+ to MO_4^{2+} reaches a value of 2, insoluble metal oxides such as $MoO_3(H_2O)$ (a hydrated form of MO_3) are obtained. This ratio of 2 (referred to in the early isopolytungstate and -molybdate literature as the *Z* value)[23] has generally defined the limits of condensed structures that span the speciation "space" between metalates (MO_4^{2-}) and solid-state MO_3.

In the present medium, not only is the acid concentration much larger than that typically used in POM synthesis, but also the medium itself is entirely different. Rather than (relatively) dilute mineral acids in water, 50% (9.4 M) aq H_2SO_4 contains ca. three molecules of water for each molecule of H_2SO_4, giving a liquid medium that may be written as, "$H_8O_3SO_4$" (Figure S15, Table S5). The data provided here argue that the thermodynamically controlled speciation chemistry of POM-component cations in this medium is dramatically different from that in water. Notably, this unique medium makes it possible to exceed the *Z* values of from 0 to 2 that have traditionally defined cluster-anion formation. As shown in eq 4, **1** reacts with H^+ in 50% H_2SO_4 to give 5 equiv of $[Mo_2O_5]^{2+}$, representing an overall *Z* value of 3 with respect to MoO_4^{2-}. (Similarly, pervanadyl, $V^{V}O_2^+$, may be viewed as the product of reacting 2 equiv of H^+ with insoluble V_2O_5.)

This access to larger *Z* values, and the larger degree of condensation inherent to the formation of $[Mo_2O_5]^{2+}$, is also due to the relative solubility and lability of Mo(VI). This contrasts with the W(VI) analogue of **1**, $H_5[PV_2W_{10}O_{40}]$, which upon mixing with 50% H_2SO_4 gave insoluble $WO_3(H_2O)$ as a yellow precipitate (which did not readily react with additional H^+).

It should be noted as well that **1** in 50% aq H_2SO_4 is quite different from **1** present as a component of the "etherate" phases used synthetically to isolate this and other cluster anions.[24] Those phases are obtained after POM formation via acid condensation in water, by adding an approximately equal volume of diethyl ether, followed by acid (HCl or H_2SO_4) to total concentrations of ca. 3 M. After mixing, the etherate phase forms as a highly dense (POM-rich) bottom layer. As part of the present work, that etherate phase was analyzed by ^{31}P NMR spectroscopy and CV (Figures S16 and S17) and, unlike in 50% aq H_2SO_4, intact **1** was the overwhelmingly dominant species present. This observation suggests that, unlike **1** in "$H_8O_3SO_4$", highly concentrated POM anions in protonated diethyl ether $[H_7C_2O]^+$ may be viewed as hybrid inorganic/organic ionic liquids.[25−27]

Finally, as is true for speciation chemistry generally, the highly condensed species present in 50% aq H_2SO_4 are formed under thermodynamic control. This not only provides for the high stability of the accessed oxidative system over cycles of reduction and reoxidation[9] but, as shown in Figure 10, also allows for facile hydrolytic assembly of intact **1** upon dilution to the less acidic aqueous environment historically more typical of polyoxometalate formation and reactivity.

CONCLUSIONS

Data provided here demonstrate that the unique medium provided by 50% aq H_2SO_4, in combination with the specific solution-state chemistry of Mo(VI), provides for the formation of more highly condensed species than typically encountered in POM cluster science. In the present case, the dissolution of $H_5[PV_2Mo_{10}O_{40}]$ (**1**; 115 mM) in 50% aqueous H_2SO_4[8,9] gives rise to phosphate, two pervanadyl ions, $V^{V}O_2^+$ (Figures 2 and 3), and 5 equiv of complexed dimolybdenum(VI) oxide, $[Mo_2O_5]^{2+}$, or closely related cations. The formation of two $V^{V}O_2^+$ ions for each equivalent of dissolved **1** is quantified by amperometric titration (Figure 4), while the formation of $[Mo_2O_5]^{2+}$-core complexes is suggested by the recovery of $[NH_4]_6[Mo_2O_5(SO_4)_4]$ (**2**) in 34% yield upon addition of $(NH_4)_2SO_4$ (Figure 8). Data from ^{31}P NMR spectroscopy additionally show that phosphate is released (Figure 5) and interacts in dynamic equilibrium with $[Mo_2O_5]^{2+}$ and possibly additional related Mo(VI) species (Figures 6 and 9).

Reactivity studies using a model reaction, the electron-transfer oxidation of *p*-xylene to *p*-methylbenzaldehyde (Figure 7), show that the impressive reactivity and selectivity of $H_5[PV_2Mo_{10}O_{40}]$ (**1**; 115 mM) in 50% aqueous H_2SO_4[8,9] arises from the combined presence of pervanadyl ions, $V^{V}O_2^+$ (with a reduction potential of 0.95 V versus Ag/AgCl), and a dynamic mixture of complexed permolybdenyl cations, $[Mo_2O_5]^{2+}$; with reduction potentials near 0 V, the permolybdenyl complexes are sufficiently reactive to plausibly provide for high selectivity by sequestering electrons from reactive organic-radical intermediates.

Finally, the acid condensation that generates $V^{V}O_2^+$ and $[Mo_2O_5]^{2+}$-core complexes upon dissolution of **1** in 50% aq H_2SO_4 is fully reversible. Upon dilution of the solution of **1** (115 mM) in 50% aq H_2SO_4 and adjustment to pH 0.8, *hydrolytically driven* assembly processes (the reverse of eq 4) lead to complete re-formation of intact **1** (Figure 10).

EXPERIMENTAL SECTION

Materials. All materials were purchased as reagent grade and used without further purification. Sodium metavanadate ($NaVO_3$, Alfa-Aesar), sodium molybdate dihydrate ($Na_2MoO_4{\cdot}2H_2O$, extra pure, Sigma-Aldrich), disodium hydrogen phosphate ($Na_2HPO_4{\cdot}9H_2O$, Bio Lab Ltd.), sodium hydroxide (NaOH, flake, 98.9% assay, Alfa Aesar), potassium bromide (KBr for IR spectroscopy, Fisher Chemical), deuterium oxide (D_2O, D, 99.9%, Tzamal D-Chem Laboratories), sulfuric acid (H_2SO_4 96%, Carlo-Erba), *p*-xylene (Sigma-Aldrich) were obtained. Additional reagent-grade salts, acids, and diethyl ether for polyoxometalate synthesis and reactions were obtained from commercial sources and used as received, except for diethyl ether, which was distilled to separate the solvent from a preservative that readily reduced the strongly oxidizing (acidic) POMs. All water used for cleaning, synthesis, and reactions was of high purity (18.2 MΩ resistivity) from a Millipore Direct-Q water purification system. The

https://dx.doi.org/10.1021/acs.inorgchem.9b03747
Inorg. Chem. 2020, 59, 11945−11952

polyoxometalates, $H_4[\alpha\text{-}PVMo_{11}O_{40}]\cdot 32.5H_2O$, $H_5[\alpha\text{-}PV_2Mo_{10}O_{40}]\cdot 34.5H_2O$, and $H_6[\alpha\text{-}PV_3Mo_9O_{40}]\cdot 34H_2O$, were prepared according to literature methods.[24] The purity of each POM was confirmed as appropriate by ^{31}P and/or ^{51}V NMR and FTIR.

Phosphorus-31 and ^{51}V NMR Experiments. Phosphorus-31 and ^{51}V NMR spectra were acquired on a Bruker 400 MHz instrument. Chemical-shift values were externally referenced to 0.24 M $Na_4P_2O_7$ (δ_p = −5.8 ppm) and 0.072 M $K_4[PVW_{11}O_{40}]$ (δ_v = −539 ppm). Internal lock signals were tuned using D_2O. Spectral data were processed using the NMR software package MestReNova.

Cyclic Voltammetry, Amperometric Titration, and Electrolysis. Cyclic voltammetry (CV) of the POMs was carried out in a three-electrodes cell setup on a CHI 760C potentiostat at 25 ± 2 °C in 0.1 M Na_2SO_4 electrolyte solutions, using a 2 mm glassy-carbon, Pt-wire, and Ag/AgCl (3 M KCl) working, counter, and reference electrodes, respectively. The scan rate was 50 mV s^{-1}.

Amperometric titrations were performed using cyclic voltammetry. **1** (115 mM) was dissolved in 9.4 M H_2SO_4 in an electrochemical cell and after its CV was recorded, increasing amounts of $NaVO_3$ (up to 230 mM) were added and cathodic-current maxima were recorded for the V^V/V^{IV} redox couple. Finally, the relative current values were plotted against the total relative concentration of V(V). A control experiment carried out starting with 230 mM $NaVO_3$ in place of 115 mM **1** gave effectively identical results.

Electrolysis in a two half-cell configurations was carried out in the presence of Pt gauze as a working electrode and Pt wire as counter and reference electrodes at 1.3 V between the anode and cathode. The two half-cells were separated by a Nafion 212 membrane washed before use with 5 wt % H_2O_2 and 8% H_2SO_4 consecutively. Prior to use, the glassy carbon working electrode was polished with 0.3 μm α-Al_2O_3 (Buehler), washed thoroughly with deionized water, and then exposed to ultrasound for approximately 5 min.

Substrate Oxidations. Typically, oxidations of *p*-xylene were carried out in 50 mL pressure tubes under N_2. The products were extracted by dichloroethane and diluted for analysis by gas chromatography (GC). The products were quantified using Thermo Scientific Focus Gas Chromatograph furnished with a dedicated flame-ionization detector (FID), and a 5% phenylmethyl silicone 0.32 mm internal diameter, 0.25 mm coating, 7 m column (Restek 5MS), using helium as the carrier gas.

Single-Crystal X-ray Measurements. A colorless block-shaped crystal (0.087 × 0.155 × 0.161 mm^3) of $[NH_4]_6[Mo_2O_5(SO_4)_4]$ was mounted on a CrystalCap ALS HT cryo-loop mount for data collection on a Rigaku XtalLAB Synergy-S single-crystal X-ray diffractometer, which includes a Hy-Pix-6000HE detector and a standard Cu Kα X-ray radiation source (λ = 1.54184 Å). Unit cell dimensions, space group assignment, data reduction, and finalization were done by using the CrysAlisPRO software package[28] (ver. 39.49, released 2018). A total of 50845 reflections were collected, of which 4578 were used after merging by SHELXL[29] according to the crystal class and on the basis of Friedel pair equivalency for structure solution. Analytical numeric absorption correction was done using a multifaceted crystal model,[30] and empirical absorption correction was done using spherical harmonics.[31] The structure was solved in the orthorhombic $C222_1$ space group (no. 20) by SHELXT[32] via intrinsic phasing and refined by SHELXL using a full-matrix least-squares technique.

The final refinement cycle included the atomic coordinates and anisotropic thermal parameters of all atoms (not including hydrogen atoms), which converged toward $R1$ = 0.0387, $wR2$ = 0.1053, and S = 1.021. All non-hydrogen atoms were located; hydrogen atoms were not assigned due to structural disorder. Full details of crystal data are listed in the Supporting Information (Table S2−S4).

Frozen-State Electron Spin Paramagnetic Resonance (ESR) Measurements. ESR measurements were carried out in a frozen state ($T \leq 100 \pm 0.1$ K) using a Bruker EMX220 X-band ($\nu \sim 9.4$ GHz) spectrometer equipped with an Oxford Instrument ESR900 cryostat and an Agilent 53150A frequency counter. Spectra processing, determination of parameters, and spectral simulations were done using the Bruker WIN-EPR/SimFonia package and OriginLab software.

■ ASSOCIATED CONTENT

Supporting Information

The Supporting Information is available free of charge at https://pubs.acs.org/doi/10.1021/acs.inorgchem.9b03747.

NMR, CV, ESR, amperometric titration, substrate oxidation, XRD, and crystal data, bond lengths and angles, and reactivity data (PDF)

Accession Codes

CCDC 1973877 contains the supplementary crystallographic data for this paper. These data can be obtained free of charge via www.ccdc.cam.ac.uk/data_request/cif, or by emailing data_request@ccdc.cam.ac.uk, or by contacting The Cambridge Crystallographic Data Centre, 12 Union Road, Cambridge CB2 1EZ, UK; fax: +44 1223 336033.

■ AUTHOR INFORMATION

Corresponding Author

Ira A. Weinstock − *Department of Chemistry and the Ilse Katz Institute for Nanoscale Science & Technology, Ben-Gurion University of the Negev, Beer Sheva 84105, Israel;* orcid.org/0000-0002-6701-2001; Email: iraw@bgu.ac.il

Authors

Chandan Kumar Tiwari − *Department of Chemistry and the Ilse Katz Institute for Nanoscale Science & Technology, Ben-Gurion University of the Negev, Beer Sheva 84105, Israel;* orcid.org/0000-0001-5470-4191

Mark Baranov − *Department of Chemistry and the Ilse Katz Institute for Nanoscale Science & Technology, Ben-Gurion University of the Negev, Beer Sheva 84105, Israel;* orcid.org/0000-0002-5517-6674

Alevtina Neyman − *Department of Chemistry and the Ilse Katz Institute for Nanoscale Science & Technology, Ben-Gurion University of the Negev, Beer Sheva 84105, Israel*

Ronny Neumann − *Department of Organic Chemistry, Weizmann Institute of Science, Rehovot, Israel 76100;* orcid.org/0000-0002-5530-1287

Complete contact information is available at: https://pubs.acs.org/10.1021/acs.inorgchem.9b03747

Notes

The authors declare no competing financial interest.

■ ACKNOWLEDGMENTS

I.A.W. and R.N. thank the Israel Ministry of Science, Technology & Space (Project 3-12589), I.A.W. thanks the Israel Science Foundation (170/17), and C.K.T. thanks the Kreitman School of Advanced Graduate Studies of Ben-Gurion University of the Negev for a doctoral fellowship. R.N. is the Rebecca and Israel Sieff Professor of Organic Chemistry and I.A.W. is the Irene Evens Professor of Inorganic Chemistry. We thank Alexander Shemes for ESR measurements.

■ REFERENCES

(1) Neumann, R. Activation of molecular oxygen, polyoxometalates, and liquid-phase catalytic oxidation. *Inorg. Chem.* **2010**, *49*, 3594−3601.

(2) Weinstock, I. A.; Schreiber, R. E.; Neumann, R. Dioxygen in polyoxometalate mediated reactions. *Chem. Rev.* **2018**, *118*, 2680−2717.
(3) Khenkin, A. M.; Neumann, R. Low-temperature activation of dioxygen and hydrocarbon oxidation catalyzed by a phosphovanadomolybdate: evidence for a Mars-van Krevelen type mechanism in a homogeneous liquid phase. *Angew. Chem., Int. Ed.* **2000**, *39*, 4088−4090.
(4) Khenkin, A. M.; Weiner, L.; Wang, Y.; Neumann, R. Electron and oxygen transfer in polyoxometalate, $H_5PV_2Mo_{10}O_{40}$, catalyzed oxidation of aromatic and alkyl aromatic compounds: Evidence for aerobic Mars-van Krevelen-Type reactions in the liquid homogeneous phase. *J. Am. Chem. Soc.* **2001**, *123*, 8531−8542.
(5) Reichert, J.; Brunner, B.; Jess, A.; Wasserscheid, P.; Albert, J. Biomass oxidation to formic acid in aqueous media using polyoxometalate catalysts - boosting FA selectivity by in-situ extraction. *Energy Environ. Sci.* **2015**, *8*, 2985−2990.
(6) Neumann, R.; Levin, M. Selective aerobic oxidative dehydrogenation of alcohols and amines catalyzed by a supported molybdenum-vanadium heteropolyanion salt $Na_5PMo_2V_2O_{40}$. *J. Org. Chem.* **1991**, *56*, 5707−5710.
(7) Sarma, B. B.; Neumann, R. Polyoxometalate-mediated electron transfer-oxygen transfer oxidation of cellulose and hemicellulose to synthesis gas. *Nat. Commun.* **2014**, *5*, 4621−4626.
(8) Sarma, B. B.; Carmieli, R.; Collauto, A.; Efremenko, I.; Martin, J. M. L.; Neumann, R. Electron transfer oxidation of benzene and aerobic oxidation to phenol. *ACS Catal.* **2016**, *6*, 6403−6407.
(9) Sarma, B. B.; Efremenko, I.; Neumann, R. Oxygenation of methylarenes to benzaldehyde derivatives by a polyoxometalate mediated electron transfer-oxygen transfer reaction in aqueous sulfuric acid. *J. Am. Chem. Soc.* **2015**, *137*, 5916−5922.
(10) Pettersson, L.; Hedman, B.; Andersson, I.; Ingri, N. Multicomponent polyanions. 34. A potentiometric and vanadium-51 NMR study of equilibria in the hydrogen(1+)-hydrogen vanadate(2-) system in 0.6 M sodium chloride medium covering the range $1 \lesssim -\lg[H+] \lesssim 10$. *Chem. Scr.* **1983**, *22*, 254−264.
(11) Pettersson, L.; Andersson, I.; Hedman, B. Multicomponent polyanions. 37. A potentiometric and vanadium-51 NMR study of equilibria in the hydrogen ion-vanadate (H^+-HVO_4^{2-}) system in 3.0 M-sodium perchlorate medium covering the range $1 \lesssim -\lg[H+] \lesssim 10$. *Chem. Scr.* **1985**, *25*, 309−317.
(12) Kozhevnikov, I. V.; Matveev, K. I. Heteropoly acids in catalysis. *Russ. Chem. Rev.* **1982**, *51*, 1075−1088.
(13) Cruywagen, J. B. B. H. a. J. J. Yellow molybdenum(VI) oxide dihydrate. *Inorganic Syntheses*; John Wiley & Sons: New York, 1986; Vol. *24*, pp 191−192.
(14) Cotton, F. A.; Morehouse, S. M.; Wood, J. S. The identification and characterization by X-ray diffraction of a new binuclear molybdenum(VI) oxalate complex. *Inorg. Chem.* **1964**, *3*, 1603−1608.
(15) Pierpont, C. G.; Buchanan, R. M. Radical-anion coordination of 9,10-phenanthrenequinone in (pentaoxo)bis(9,10-phenanthrenequinone)dimolybdenum. *J. Am. Chem. Soc.* **1975**, *97*, 6450−6455.
(16) Pierpont, C. G.; Buchanan, R. M. Molybdenum complexes containing catecholate ligands. Structural studies on complexes of the pentaoxobis(quinone)dimolybdenate(n-) (n = 0, 1, 2) redox series. *Inorg. Chem.* **1982**, *21*, 652−657.
(17) Burgmayer, S. J. N.; Stiefel, E. I. Synthesis and structure of the first molybdenum-pterin complex. *J. Am. Chem. Soc.* **1986**, *108*, 8310−8311.
(18) Malinak, S. M.; Coucouvanis, D. Synthesis and characterization of $[Mo_2O_5]^{2+}$-bridged complexes containing cofacially-oriented, catechol-functionalized macrocyclic and SALPHEN ligands. *Inorg. Chem.* **1996**, *35*, 4810−4811.
(19) Malinak, S. M.; Rosa, D. T.; Coucouvanis, D. A new class of complexes possessing cofacially-oriented, planar, metal-containing subunits. synthesis, characterization, and reactivity of $[(MoO_2)_2(\mu\text{-}O)]^{2+}$-linked, catechol-functionalized, tetraazamacrocyclic and salicylideneamine complexes. *Inorg. Chem.* **1998**, *37*, 1175−1190.
(20) Neves, P.; Gago, S.; Balula, S. S.; Lopes, A. D.; Valente, A. A.; Cunha-Silva, L.; Paz, F. A. A.; Pillinger, M.; Rocha, J.; Silva, C. M.; Gonçalves, I. S. Synthesis and catalytic properties of molybdenum(VI) complexes with tris(3,5-dimethyl-1-pyrazolyl)methane. *Inorg. Chem.* **2011**, *50*, 3490−3500.
(21) Goldberg, H.; Kaminker, I.; Goldfarb, D.; Neumann, R. Oxidation of carbon monoxide cocatalyzed by palladium(0) and the $H_5PV_2Mo_{10}O_{40}$ polyoxometalate probed by electron paramagnetic resonance and aerobic catalysis. *Inorg. Chem.* **2009**, *48*, 7947−7952.
(22) Pettersson, L.; Andersson, I.; Grate, J. H.; Selling, A. Multicomponent Polyanions. 46. Characterization of the isomeric keggin decamolybdodivanadophosphate ions in aqueous solution by ^{31}P and ^{51}V NMR. *Inorg. Chem.* **1994**, *33*, 982−993.
(23) Pope, M. T. *Heteropoly and Isopoly Oxometalates.*; Springer: Berlin, 1983.
(24) Tsigdinos, G. A.; Hallada, C. J. Molybdovanadophosphoric acids and their salts. I. Investigation of methods of preparation and characterization. *Inorg. Chem.* **1968**, *7*, 437−441.
(25) Chiang, M.-H.; Dzielawa, J. A.; Dietz, M. L.; Antonio, M. R. Redox chemistry of the Keggin heteropolyoxotungstate anion in ionic liquids. *J. Electroanal. Chem.* **2004**, *567*, 77−84.
(26) Bernardini, G.; Wedd, A. G.; Zhao, C.; Bond, A. M. Photochemical oxidation of water and reduction of polyoxometalate anions at interfaces of water with ionic liquids or diethylether. *Proc. Natl. Acad. Sci. U. S. A.* **2012**, *109*, 11552−11557.
(27) Misra, A.; Franco-Castillo, I.; Müller, D. P.; González, C.; Eyssautier-Chuine, S.; Ziegler, A.; de la Fuente, J. M.; Mitchell, S. G.; Streb, C. Polyoxometalate-ionic liquids (POM-ILs) as anticorrosion and antibacterial coatings for natural stones. *Angew. Chem., Int. Ed.* **2018**, *57*, 14926−14931.
(28) Rigaku. *CrysAlis PRO*; Rigaku Oxford Diffraction: Yarnton, England, 2018.
(29) Sheldrick, G. M. Crystal structure refinement with SHELXL. *Acta Crystallogr., Sect. C: Struct. Chem.* **2015**, *71*, 3−8.
(30) Clark, R. C.; Reid, J. S. The analytical calculation of absorption in multifaceted crystals. *Acta Crystallogr., Sect. A: Found. Crystallogr.* **1995**, *51*, 887−897.
(31) *SCALE3 ABSPACK - An Oxford Diffraction program (1.0.4)*; Oxford Diffraction Ltd., 2005.
(32) Sheldrick, G. SHELXT - Integrated space-group and crystal-structure determination. *Acta Crystallogr., Sect. A: Found. Adv.* **2015**, *71*, 3−8.

https://dx.doi.org/10.1021/acs.inorgchem.9b03747
Inorg. Chem. 2020, 59, 11945−11952